Journal of Power Sources 196 (2011) 8116–8124

Contents lists available at ScienceDirect

Journal of Power Sources

journal homepage: www.elsevier.com/locate/jpowsour

A study of lithium ion intercalation induced fracture of silicon particles used as anode material in Li-ion battery

S. Kalnaus [a,*], K. Rhodes [b], C. Daniel [a,b]

[a] Materials Science and Technology Division, Oak Ridge National Laboratory, One Bethel Valley Road, P.O. Box 2008, MS-6083, Oak Ridge, TN 37831-6083, USA
[b] Department of Materials Science and Engineering, University of Tennessee, Knoxville, TN 37996-2200, USA

ARTICLE INFO

Article history:
Received 3 March 2011
Received in revised form 17 May 2011
Accepted 19 May 2011
Available online 27 May 2011

Keywords:
Lithium ion battery
Anode
Damage
Fracture

ABSTRACT

The fracture of Si particles due to internal stresses formed during the intercalation of lithium ions was described by means of a thermal analogy model and brittle fracture damage parameter. The stresses were calculated following the diffusion equation and equations of elasticity with an appropriate volumetric expansion term. The results were compared with the acoustic emission data from the experiments on electrochemical cycling of Li ion half-cells with silicon electrodes. A good correlation between experiment and prediction was observed. The results of computations with different particle sizes show the existence of a critical size below which fracture during the lithiation is not expected to occur. Such a critical size appears to be within micrometer scale.

1. Introduction

Electrification of automotive drivetrains or powertrains is one of the primary research directions for the reduction of petroleum dependence. Lithium ion based electrochemical energy storage technology is the primary candidate for plug-in hybrid electric vehicles (PHEV) and fully electric vehicles (EV), and an ongoing collaborative research between companies and research institutions provides evidence for a high potential of application of Li-ion batteries in vehicle development. Despite attractive features and wide range of applications in smaller scale devices such as consumer electronics, the service life of Li-ion battery systems is still limited due to the processes of degradation of electrode material with repeated charging and discharging, and mechanisms of such degradation have not been sufficiently investigated and understood.

The working principle of Li ion battery is based on repeated transport of lithium ions through electrolyte and insertion/extraction from the electrode host structure (intercalation compound). It has been well documented that cycles of charge and discharge lead to capacity fade in a battery over its lifetime [1–3]. Such capacity fade is suggested to be partially attributed to mechanical cracking of the active material particles induced by repeated lithium intercalation/deintercalation [4]. While the fracture of particles has been observed and documented, investigation of processes leading to crack formation and development of models capable of predicting initiation of cracking is still under way [5]. It should be mentioned that historically the area of battery research was driven predominantly by electrochemical expertise and materials development. This resulted in an enormous gap in research on mechanical behavior of electrode materials. At the present stage it is evident that the mechanical engineering side of the problem needs to be explored. Determination of the stress state of a particle during charge/discharge will lead to understanding the origin of fracture and will provide a solution in order to improve the battery service life.

It is well known that electrochemical cycling leads to capacity fade in lithium ion batteries, which creates significant limitations as far as lifetime and reliability of a product is concerned [1,2]. In addition to processes associated with chemical reactions, a major source of capacity fade is the failure of electrode particles due to the stresses developed during lithium intercalation/deintercalation. Higher lithium insertion rates generally result in higher rate of fracture due to significant lattice strain [5]. There is a multitude of experimental evidence supporting the notion of active electrode particle failure due to intercalation stresses [6–9]. The process of cyclic expansion and contraction of active electrode material can be viewed from the standpoint of fatigue and damage mechanics. However, to the present day, the term “mechanical fatigue” has rarely been applied to the processes involved in electrochemical cycling.

Involvement of mechanical stresses in battery degradation has been realized only recently and the modeling efforts have started utilizing a combination of diffusion laws with continuum mechanics [10–15]. Most known is the thermal analogy approach

* Corresponding author. Tel.: +1 865 576 6181; fax: +1 865 574 4357.
E-mail address: kalnauss@ornl.gov (S. Kalnaus).

0378-7753/$ – see front matter © 2011 Elsevier B.V. All rights reserved.
doi:10.1016/j.jpowsour.2011.05.049

Nomenclature

c	lithium concentration
D	damage parameter
D_{Li}	diffusion coefficient
e	dilatational strain
E	modulus of elasticity
$\tilde{E}^+$	modulus of elasticity in tension
$\tilde{E}^-$	modulus of elasticity in compression
F	Faraday constant
h	material constant related to partial closure of micro defects
i_s	surface current density
J	flux
m	Weibull modulus
P_{f1}	probability of fracture
r	radial coordinate
R	gas constant
R_0	radius of the particle
t	time variable
T	temperature
α	coefficient of thermal expansion
δ_{ij}	Kronecker delta
ε_{ij}	components of strain tensor
ε_r	radial component of strain
ε_t	tangential component of strain
$\vec{\eta}_k$	k-th eigenvector of stress tensor
ν	Poisson ratio
σ_{sq}	equivalent stress
σ_H	hydrostatic stress
σ_{ij}	components of stress tensor
σ_k	k-th eigenvalue of stress tensor
σ_r	radial component of stress
σ_t	tangential component of stress
σ_{VM}	Von Mises stress
σ_w	Weibull stress
$\langle\sigma\rangle_{ij}^+$	positive part of stress tensor
$\langle\sigma\rangle_{ij}^-$	negative part of stress tensor
χ	triaxiality parameter
Ω	partial molar volume
$\mathrm{tr}(\sigma)$	trace of tensor σ
$\langle\cdot\rangle$	Macauley bracket

developed by Yang [10] for calculation of chemical stresses, which has been adopted in subsequent investigations [11–13]. The idea of description of volumetric expansion due to diffusion based on equations of thermal expansion is rather appealing due to simplicity of elastic equations and this approach is used in the current work. Computations based on such approach can give a good approximation of stress distribution, provided an appropriate diffusion law is available.

The electrochemical cycling of the electrochemical cell imposes cycles of expansion and contraction similar to repeated cycles of thermal straining. Following the analogy, the notion of thermal fatigue could be applied to failure of electrode material. The phenomenon of thermal fatigue has been investigated over a long period of time [16–18] and the presence of temperature induced plastic deformation in ductile materials has been reported [16]. In such cases the relation between accumulation of damage and plastic strain energy results in the fatigue criterion for life prediction [19–21]. The majority of Li-ion battery electrode materials (Si, $LiMn_2O_4$, $LiCoO_2$, representing the typical anode and cathode compounds) are however brittle in nature and the accumulation of damage in this case is best described by the change in elastic properties due to formation of microcracks. When the microcracks reach the critical size (typically very small compared to critical cracks in ductile materials) complete failure occurs. In this regard the damage can be related to the fraction of Young's modulus available for further elastic deformation and the value of modulus equal to zero would represent complete fracture. Development of the relationship between the stress state and damage parameter cannot be based on Von Mises stress, as in case of ductile materials, and should include a different formulation of equivalent stress [22,23].

The present work represents investigation of fracture in Si particles used as an active material for anodes in a Li-ion battery. Without venturing into details of electrochemical aspects of battery operation, the problem is treated from the stress analysis point of view. The results are compared with the acoustic emission data from Si electrode cycling and a good correlation was found between the peak of emissions and the predicted time when the damage parameter reaches its maximum.

2. Evaluation of intercalation induced stress

The overall problem of ionic diffusion in solid particles is very complex from both electrochemical and mechanical points of view and therefore necessary approximations are made to reflect particular aspects of the overall process. By considering binary diffusion coefficients and thermodynamic driving force for diffusion, Newman and Christensen [14,15] developed a continuum model for computation of internal stresses in a spherical particle of cathode material. Another approach is based on a rather natural analogy between volumetric thermal expansion and three-dimensional diffusion [10–13]. The following section provides brief description of the thermal analogy model in terms of mathematical formulation within continuum mechanics framework. The particle is approximated as a homogenous isotropic sphere for simplicity. The process of Li-ion solid state diffusion is considered as a process analogous to the thermal expansion of a homogeneous sphere submerged into liquid media which has higher temperature than the sphere. The elastic thermal analysis of an isotropic media is governed by Hooke's law with additional thermal expansion term [24]

$$\varepsilon_{ij} = \frac{1}{E}[(1+\nu)\sigma_{ij} - \nu\sigma_{kk}\delta_{ij}] + \alpha\,\Delta T\delta_{ij} \tag{1}$$

Dummy index summation convention is used in Eq. (1) with δ_{ij} being Kronecker delta, ε_{ij} and σ_{ij} represent strain and stress tensor components, respectively, ν is the Poisson ratio, α is the coefficient of thermal expansion, and ΔT represents temperature change at the material point. Analogous to Eq. (1) the bulk diffusion in isotropic media can be represented by the following stress–strain relationship [10]

$$\varepsilon_{ij} = \frac{1}{E}[(1+\nu)\sigma_{ij} - \nu\sigma_{kk}\delta_{ij}] + \frac{\Delta c\Omega}{3}\delta_{ij} \tag{2}$$

where Ω is the partial molar volume and c is the concentration of diffusing species at the material point. Since Ω is a volumetric quantity it can be determined analogously to volumetric coefficient of thermal expansion as

$$e = \Omega\,\Delta c \tag{3}$$

where $e = \varepsilon_{kk}$ is the volumetric strain.

The case of the spherical geometry of a particle produces only two components of the stress tensor in spherical coordinates: radial component (σ_r) and tangential component (σ_t). The equilibrium condition for the stress tensor in case of a spherical particle reduces to

$$\frac{d\sigma_r}{dr} + \frac{2}{r}(\sigma_r - \sigma_t) = 0 \tag{4}$$

The stresses are functions of elastic strains following the Hooke's law

$$\begin{cases} \sigma_r = \dfrac{E}{(1+\nu)(1-2\nu)}\left[(1-\nu)\varepsilon_r + 2\nu\varepsilon_t - (1+\nu)\dfrac{\Omega c}{3}\right] \\ \sigma_t = \dfrac{E}{(1+\nu)(1-2\nu)}\left[\nu\varepsilon_r + \varepsilon_t - (1+\nu)\dfrac{\Omega c}{3}\right] \end{cases} \tag{5}$$

where the components of strain are determined from the radial displacement as

$$\varepsilon_r = \frac{dU}{dr} \qquad \varepsilon_t = \frac{U}{r} \tag{6}$$

Substitution of Eq. (6) in expressions for stress (5) and then to equilibrium Eq. (4) leads to the ordinary differential equation for displacement as a function of radial coordinate r

$$\frac{d^2U}{dr^2} + \frac{2}{r}\frac{dU}{dr} - \frac{2U}{r^2} = \frac{1+\nu}{1-\nu}\frac{\Omega}{3}\frac{dc}{dr} \tag{7}$$

Provided the instantaneous concentration of diffusing species is known, solution of Eq. (7) with back substitution in Eqs. (6) and (5) gives the stress state within the particle.

The diffusion equation is introduced as an extension of the Fick's law with the component corresponding to diffusion driven by the hydrostatic stress σ_H [10,11]

$$\frac{\partial c}{\partial t} = D_{\mathrm{Li}}\nabla^2 c - \frac{D_{\mathrm{Li}}\Omega}{RT}(\nabla c \nabla\sigma_H + c\nabla^2\sigma_H) \tag{8}$$

where D_{Li} is the diffusion coefficient, R is the gas constant, T is the absolute temperature, and $\sigma_H = \sigma_{kk}/3$ is hydrostatic stress. When dependence on radial coordinate r only is considered, as in the case of isotropic spherical particle with uniform distribution of solute at the surface, the diffusion equation becomes

$$\frac{\partial c}{\partial t} = D_{\mathrm{Li}}\left[\frac{\partial^2 c}{\partial r^2} + \frac{2}{r}\frac{\partial c}{\partial r} - \frac{\Omega}{RT}\frac{\partial c}{\partial r}\frac{\partial\sigma_H}{\partial r} - \frac{\Omega c}{RT}\left(\frac{\partial^2\sigma_H}{\partial r^2} + \frac{2}{r}\frac{\partial\sigma_H}{\partial r}\right)\right] \tag{9}$$

Eqs. (5)–(7) together with the diffusion equation (Eq. (9)) describe the problem of ionic diffusion in a homogenous spherical particle. In fact, Eq. (7), being an ordinary differential equation, can be solved analytically which results in the following expressions for stress components

$$\begin{cases} \sigma_r = \dfrac{2\Omega E}{3(1-\nu)}\left[1/R_0^3\displaystyle\int_0^{R_0} cr^2\,dr - 1/r^3\int_0^r cr^2\,dr\right] \\ \sigma_t = \dfrac{\Omega E}{3(1-\nu)}\left[2/R_0^3\displaystyle\int_0^{R_0} cr^2\,dr + 1/r^3\int_0^r cr^2\,dr - c\right] \end{cases} \tag{10}$$

where R_0 is the radius of the particle. After substituting $\sigma_H = (\sigma_r + 2\sigma_t)/3$ with stress components expressed in Eqs. (9) and (10) the differential equation for concentration evolution becomes

$$\frac{\partial c}{\partial t} = D_{\mathrm{Li}}\left(\frac{\partial^2 c}{\partial r^2} + \frac{2}{r}\frac{\partial c}{\partial r} + \theta\left(\frac{\partial c}{\partial r}\right)^2 + \theta c\left(\frac{\partial^2 c}{\partial r^2} + \frac{2}{r}\frac{\partial c}{\partial r}\right)\right), \qquad \theta = \frac{2\Omega^2 E}{9RT(1-\nu)} = \text{const.} \tag{11}$$

Eq. (11) represents a boundary-initial value problem and can be solved numerically on the one-dimensional space grid. It should be mentioned, that the statement of the problem in form of Eqs. (10) and (11) is performed based on the assumption of instantaneous mechanical response, i.e. the stress–strain state depends on time only implicitly via concentration function $c(r, t)$. At each particular time step during electrochemical cycling process, the Eq. (11) is solved first and the stresses are obtained as a function of radial coordinate by integration of Eq. (10). The values of concentration of Li ions from the previous time step serve as initial conditions for the numerical procedure at the next time step. The boundary condition imposed at the surface of the particle is controlled by the current density as [11]

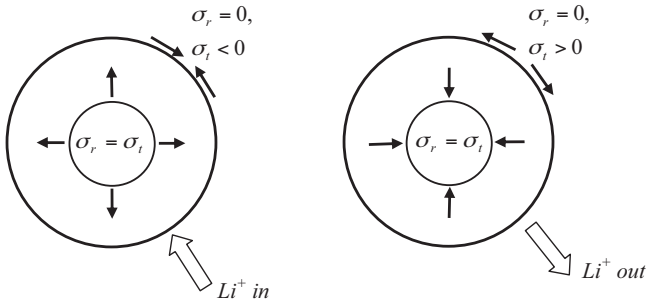

Fig. 1. Schematics of intercalation/deintercalation stresses in a spherical particle.

$$J = -D_{\mathrm{Li}}\left(\nabla c - \frac{\Omega c}{RT}\nabla\sigma_H\right)\Big|_{r=R_0} = \frac{i_S}{F} \tag{12}$$

where F is the Faraday constant, J is the species flux and i_s is the current density at the surface of the particle. Considering solution for stresses (Eq. (10)) this boundary condition becomes

$$J = -D_{\mathrm{Li}}(1+\theta c)\frac{\partial c}{\partial r}\Big|_{r=R_0} = \frac{i_S}{F} \tag{13}$$

The second boundary condition reflects the symmetry of concentration distribution with respect to the center of the particle and is represented by the equation

$$\frac{\partial c}{\partial r}\Big|_{r=0} = 0 \tag{14}$$

3. Damage and brittle fracture

Eq. (11) with the boundary conditions stated in Eq. (13) and Eq. (14) describes the evolution of concentration of Li ions in a solid homogenous spherical particle with time, following the cyclic charge/discharge curve. Such a curve is typically given as a current (voltage) versus time diagram of an electrochemical cell. By solving Eq. (11) the concentration as a function of a radial coordinate is found at a particular time and the stresses are obtained by integration of expressions in Eq. (10). Thus the stress distribution is obtained.

The above procedure is based on the analogy of chemical diffusion stresses to the thermal stresses in continuum mechanics. In the case of ductile materials, the thermal cyclic loading is known to contribute to the fatigue damage accumulation governed by cyclic plasticity [16–18]. Many of the typical active electrode materials in lithium chemistries are brittle in nature, such as $LiCoO_2$, $LiMn_2O_4$, and Si. Therefore the damage parameter cannot be based on accumulated plastic strain energy as in the case of ductile engineering materials [21–23]. Electrode material deforms volumetrically with cyclic insertion and removal of Li ions from its crystallographic structure. Such cycles of lithiation/delithiation produce corresponding compressive and tensile stresses within a particle, as schematically illustrated in Fig. 1.

The representation of strength of brittle materials (e.g. ceramic) is not deterministic in nature and follows the Weibull distribution [25,26]. The assessment of tensile strength is based on the results of load-to-rupture tests performed on large set of specimens with application of corresponding statistical analysis [27]. The likelihood of fracture is governed by the distribution of flaws in the specimen and is based on the weakest link approach. The distribution of flaws

is assumed to be stable and no slow crack growth is occurring during the loading [27]. In this case the probability of fracture of a specimen subject to tensile stress σ is represented as [26]

$$P_{f1} = 1 - e^{-(\sigma/\sigma_W)^m} \tag{15}$$

where σ_W and m are the Weibull stress and the Weibull modulus correspondingly determined from the series of load-to-rupture experiments.

The process of material deformation as a result of ionic diffusion is a time-dependent process which changes material itself and thus the assumption that the initial population of internal flaws does not change with time is no longer valid. Formulation for damage accumulation as the material is subject to rising stresses due to species concentration gradients is done adopting a quasi-brittle approach [26,28,29]. In case of uniaxial loading, the damage D is described as the ratio of the failed area of the sample to the original area. If the specimen is represented as an assembly of N identical fibers out of which n have failed at a given time increment, then the damage is n/N and represented by Eq. (15). The effective tensile stress resulting from the re-distribution of load due to reduction in load-bearing area is then $\tilde{\sigma} = \sigma/(1-D)$. The effective compressive stress is $\tilde{\sigma} = \sigma/(1-hD)$ and the constant h reflects the partial recovery of elasticity in compression due to closure of micro-cracks. The effective Young's modulus in tension and compression is represented as

$$\begin{cases} \tilde{E}^+ = E(1-D) \\ \tilde{E}^- = E(1-hD) \end{cases} \tag{16}$$

and the constant h is therefore $h = (E - \tilde{E}^-)/(E - \tilde{E}^+)$. For most materials, the ratio h has a value close to 0.2 [26] and this value is adopted in the present investigation.

The above reasoning can be extended to the case of multiaxial stress state in which case the effective stress tensor is introduced. The positive and negative parts of a stress tensor are constructed from its positive (negative) eigenvalues σ_k and corresponding eigenvectors $\vec{\eta}^k$ as follows

$$\begin{aligned} \langle \boldsymbol{\sigma} \rangle_{ij}^+ &= \sum_{k=1}^{3} \left\langle \boldsymbol{\sigma}_k \right\rangle \eta_i^k \eta_j^k \\ \langle \boldsymbol{\sigma} \rangle_{ij}^- &= \boldsymbol{\sigma}_{ij} - \langle \boldsymbol{\sigma} \rangle_{ij}^+ \end{aligned} \tag{17}$$

where $\langle\rangle$ represents Macauley brackets such that $\langle x \rangle = \begin{cases} x, \text{ if } x \geq 0 \\ 0, \text{ if } x = 0 \end{cases}$.

The above definition results in the following expression for the effective stress tensor in multiaxial stress state

$$\tilde{\sigma}_{ij} = \frac{\langle \boldsymbol{\sigma} \rangle_{ij}^+}{1-D} + \frac{\langle \boldsymbol{\sigma} \rangle_{ij}^-}{1-hD} + \frac{\nu}{1-2\nu} \left(\frac{\delta_{kl} \langle \boldsymbol{\sigma} \rangle_{kl}^+ - \langle \sigma_{kk} \rangle}{1-D} + \frac{\delta_{kl} \langle \boldsymbol{\sigma} \rangle_{kl}^- + \langle -\sigma_{kk} \rangle}{1-hD} \right) \delta_{ij} \tag{18}$$

As for the damage parameter under multiaxial stress, the quantity σ in Eq. (15) should be substituted with a corresponding equivalent stress parameter representing the current stress state. Thus the damage parameter becomes represented by

$$D = 1 - e^{-(\sigma_{eq}/\sigma_W)^m} \tag{19}$$

We choose the equivalent stress definition in form that depends on the hydrostatic stress [26]

$$\begin{aligned} \sigma_{eq} &= \sigma_{VM} \sqrt{\chi} \\ \chi &= \frac{2}{3}(1+\nu) + 3(1-2\nu)\left(\frac{\sigma_H}{\sigma_{VM}} \right)^2 \end{aligned} \tag{20}$$

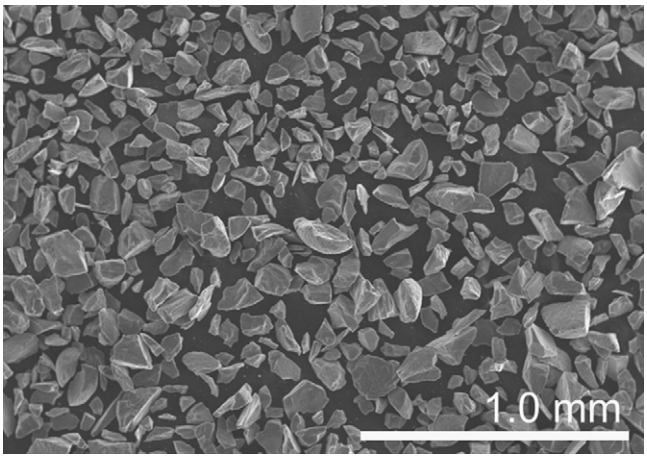

Fig. 2. Si particles used in the experiments.

where σ_{VM} is the Von Mises stress and χ is the triaxiality parameter. With inclusion of elasticity change due to damage the equivalent stress is expresses by

$$\sigma_{eq} = \sqrt{(1+\nu)\langle \boldsymbol{\sigma} \rangle_{ij}^+ \langle \boldsymbol{\sigma} \rangle_{ij}^+ - \nu \langle tr\boldsymbol{\sigma} \rangle^2 + \frac{1-D}{1-hD} \left[(1+\nu)\langle \boldsymbol{\sigma} \rangle_{ij}^- \langle \boldsymbol{\sigma} \rangle_{ij}^- - \nu \langle -tr\boldsymbol{\sigma} \rangle^2 \right]} \tag{21}$$

It can be seen that the damage evolution and stress state are interrelated by Eqs. (19) and (21) via the equivalent stress parameter. The overall solution procedure can be described as follows. The electrochemical "loading curve" is represented by the variation of current with time. At the initial moment the initial concentration of Li inside the particle is known and the stresses can be obtained from Eq. (10). The initial damage is taken to be zero and then corrected by Eq. (19) using the equivalent stress from Eq. (21). The solution is continued following the same steps for each point along the current versus time curve. Following the assumption of isotropic material, the damage is isotropic as well and represented by one scalar variable.

4. Comparison with experimental data

In the present section the computational results of the damage accumulation are compared to the results of acoustic emission (AE) experiments on anodes with Si active material. A series of experiments were conducted on lithium half cells with Li counter electrode under different charge/discharge conditions. The silicon particles (−100/+325 mesh from Alfa Aesar) were mixed with 10 wt% PVDF binder and 10 wt% carbon black as conductive additive, and spread over copper circular disks with radius equal to 12 mm. The surface density of Si was 2.5 mg/cm^2. Silicon particles in as received condition are shown on the SEM picture in Fig. 2. The average size of the particles was 100 μm.

The half cell employed in the experiments consisted of two stainless steel plates and insulating PTFE gasket in which the Si composite anode, separator and Li foil were placed. A 1 M solution of $LiPF_6$ in ethylene carbonate and ethyl methyl carbonate (3:7 wt) (Ferro Corp.) was used as electrolyte. The half cells were cycled using Maccor battery tester. The AE data was collected using a 4 channel system from Physical Acoustics.

The experiments were conducted under constant current–constant voltage (CCCV) conditions with corresponding cut-off values. CCCV process consists of periods of time when the cell is held at constant current until the voltage reaches desired cut-off value and then the cell is held at constant voltage until the current drops to the designed value. The details of CCCV procedure can be found in [30,31]. The representative cyclic curve is shown in

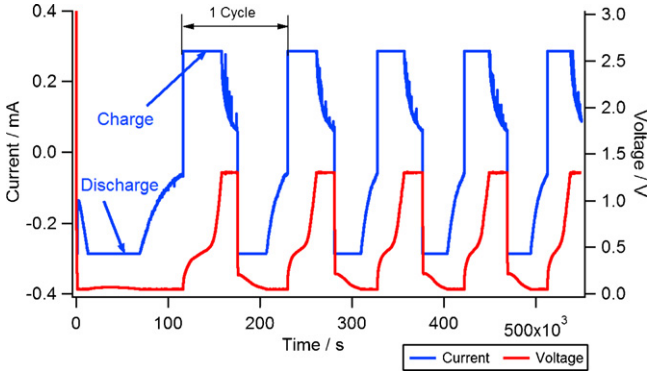

Fig. 3. Example of constant current–constant voltage cycling curve used in the experiments.

Fig. 3. Total of eleven cells with Si anodes were cycled with current amplitudes ranging from 0.29 to 2.3 mA.

In order to eliminate noise, acoustic emissions representing particle cracking were filtered based on 21 dB threshold. The electromagnetic interference (EMI) events were registered by an additional AE sensor placed near the cell and these events were filtered out. The acoustic emission parameters (i.e. duration, amplitude and frequency) were compared to those available in the literature [32–34] and a good agreement was observed. The details of signal collection and post-processing can be found in corresponding Refs. [31–34].

Determination of several material constants is required in order to use the equations specified above. The partial molar volume was determined based on the analogy with volumetric coefficient of thermal expansion. The volumetric strain (e_T) due to the temperature change ΔT is expressed as $e_T = \alpha_V \Delta T$, where α_v is the volumetric coefficient of thermal expansion. Analogously, for volumetric expansion due to intercalation of lithium, $e_C = \Omega \Delta C$, where ΔC is the change in lithium concentration. Based on 300% volume increase in Li_xSi when x changes from 0 to 4.4 [30] the value of Ω is 7.69×10^{-6} m^3 mol^{-1}. In the current work the diffusion coefficient is assumed to be constant and independent of state of charge (stress state). The parameters of Weibull distribution for strength of Si were adopted from the literature [25]. The apparent value of the diffusion coefficient and other material constants is shown in Table 1 together with corresponding references reporting these values.

The solution of the diffusion equation (Eq. (11)) is controlled by the surface current density boundary condition (Eq. (13)). At each point in time, the current density at the particle surface was obtained by dividing the total current by the average number of Si particles in the electrode and by the average surface area of a particle. Thus each point from the current cycling curve (Fig. 3) can be converted to an average surface current density of a particle. Each time interval from the cycling electrical data was split into sub-intervals for time integration of Eq. (11). The numerical solution of initial-boundary value problem was performed by backward time centered space (BTCS) method. The overall arrangement of the solution steps is shown in Table 2, where indexes k and l indicate time step and node numbers respectively. The primary interests were the evolution of maximum damage within a particle with time, distribution of stress and distribution of damage inside the particle. Influence of cycling conditions on damage development was investigated. The results are compared with experimental AE data records of cracking events.

Table 1
Material properties used in calculations.

D_{Li} m^2 s^{-1}	Ω m^3 mol^{-1}	E GPa	ν	σ_w GPa	m	ρ kg m^{-3}
5.1×10^{-16} [36–39]	7.69×10^{-6} [30]	190 [25,35]	0.218 [35]	6.1 [25]	3.6 [25]	2.33×10^3 [35]

Table 2
Solution steps for determination of damage parameter.

1 Input cyclic curve I_k, t_k
2 $t = 0$, $D_0 = 0$, $c_{0l} = 0$
3 For each t_k:
3.1 Obtain $i_s^{(k)}$ for BC Eq. (13)
3.2 Solve FDE form of Eq. (11) for nodal c_{kl} (Thomas algorithm is used for tridiagonal matrix).
3.3 $\sigma^{(k,l)}$ – Eq. (10)
3.4 $\sigma_{eq}^{(k,l)}$ – Eq. (21)
3.5 $D_{k,l}$ – Eq. (19)
3.6 Search for max D_k
3.7 $t = t_k + \Delta t$ and go to 3.1

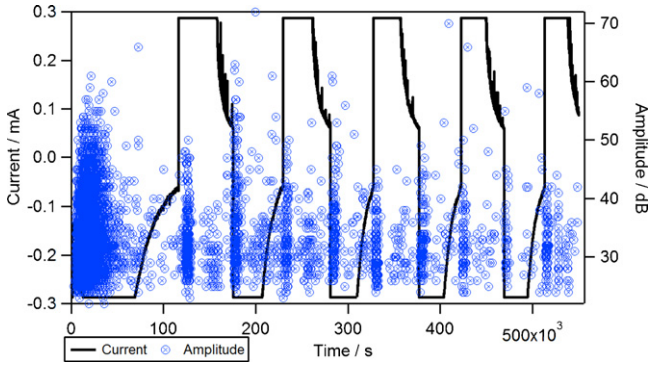

Fig. 4. AE data for electrochemical cycling of Si anode: specimen ID 48.

As an example, the acoustic emission data for a representative specimen (sample ID 48) is shown in Fig. 4 together with the cyclic current as a function of time. The markers represent the amplitude of the acoustic events (hits) distributed within the duration of experiment. It can be seen that most of the cracking associated with the AE hits occurs during the first discharge, i.e. at the beginning of the first cycle. This situation appears to be typical for all of the specimens investigated. The subsequent emissions registered at the beginning of the corresponding charge (positive current) and discharge (negative current) portions of the cyclic curve can be attributed to the formation of new cracks within the grains fractured during the first cycle. The influence of the newly created cracks on the electrochemical and mechanical properties of the particle is beyond the scope of current investigation. At the present stage it appears to be essential to verify that the approach described above can predict the fracture of particle in agreement with the acoustic emission data during the first cycle. That is the "safe-life" approach is taken and only the accumulation of damage in the initially not fractured particle is considered. Under this condition, the first maximum of emission rate should coincide with the maximum of the damage parameter.

The damage evolution with time is shown together with the rate of emissions in Fig. 5 for the specimen ID 48. Only the first discharge portion of the cycle is shown. Since the silicon electrode is cycled against lithium, the former becomes a cathode in the half-cell and the intercalation of Li ions occurs during discharge. The dash-dotted line in Fig. 5 represents the rate of the emissions collected during the experiment and the solid line represents the calculated damage based on the current evolution in time. Emission rate was calculated by differentiating the number of events versus time data. The data is most successfully fitted with the Hill equation

$$F(x) = b + \frac{m - b}{1 + (I_h/x)^r} \tag{22}$$

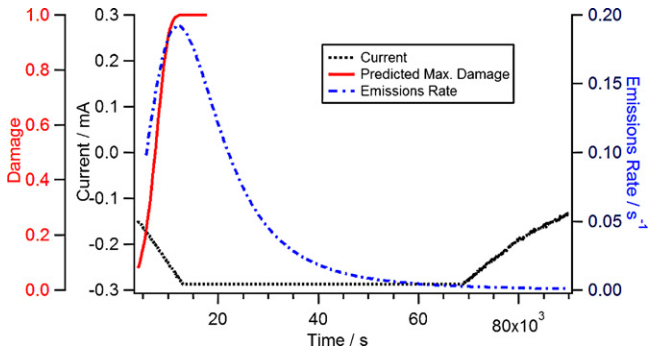

Fig. 5. Correlation between emissions rate from experiment and computed evolution of maximum damage.

where b, m, I_h, and r are fitting parameters. The point where the rate of acoustic emission events reaches its maximum is considered to be the point where most of the particles within electrode experience fracture.

With the use of the damage parameter, the time when $D = 1$ represents the time to failure of a particle. It can be seen from Fig. 5 that the maximum of damage parameter (value of 1.0) correlates well with the maximum of emissions rate.

The correlation between experimental data and predicted fracture based on $D = 1$ criterion is shown in Fig. 6. The markers represent data for individual specimens. The solid line indicates perfect correlation and dashed lines show the boundary within the factor-of-two dispersion from the perfect correlation. It can be seen that the experimental data is in good agreement with computed values of time to failure based on the brittle damage parameter.

Out of eleven specimens under investigation, ten were cycled between 1.3 V and 50 mV under different cut-off currents. One specimen was tested with higher cut-off voltage, and cycled between 1.3 and 170 mV. The particles in this electrode did not fracture and no acoustic emission was detected during cycling. This specimen is indicated by an arrow in Fig. 6 implying that the electrode particles did not fail. An arbitrary time of 80×10^4 s was

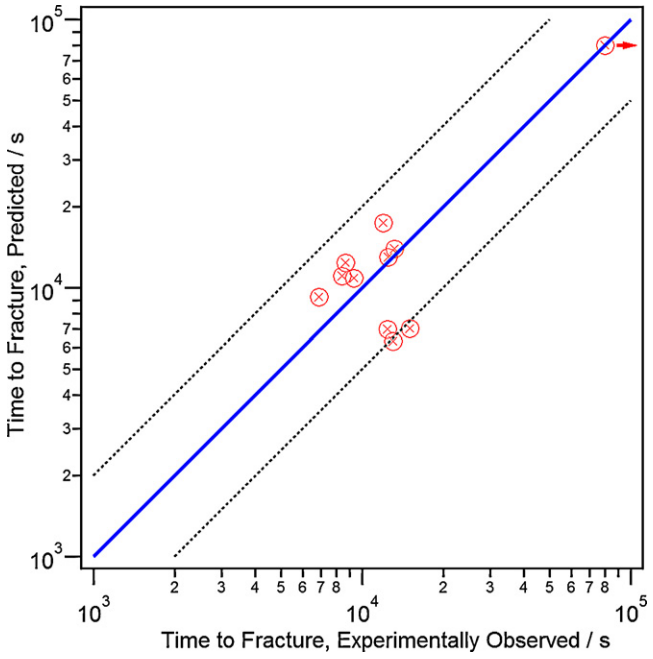

Fig. 6. Correlation between observed and predicted fracture times; an arrow next to the data point indicates that no fracture was observed.

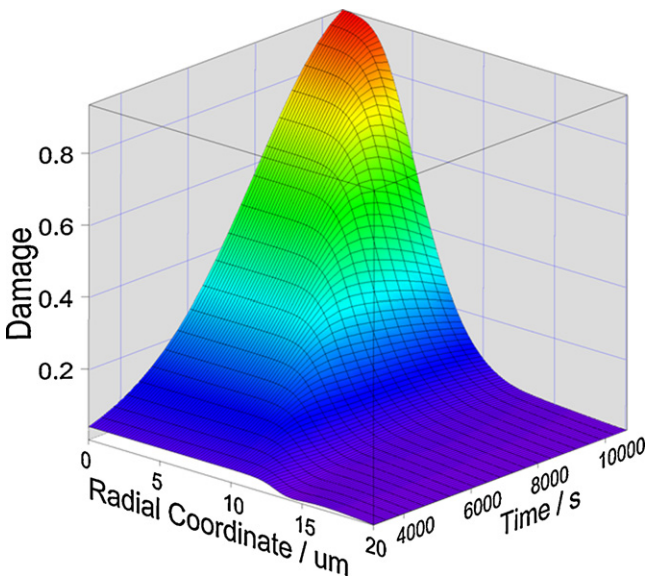

Fig. 7. Computed damage evolution as a function of time and radial coordinate of a spherical particle.

chosen to represent the infinite time to fracture. Higher cut-off voltage resulted in only partial lithiation of Si which reduced the internal stresses within particles thus reducing the damage. The maximum damage in this specimen reached the value of 0.15 only, therefore predicting the experimentally observed non-failure.

In Fig. 5 the maximum value of damage within the particle is shown for each corresponding moment of time. The distribution of damage within the particle is of particular interest since the location of its maximum would represent the point where the fatal crack originates. The damage as a function of the radial coordinate and time ($D(r,t)$) is plotted in Fig. 7. The three-dimensional representation in Fig. 7 depicts the evolution of damage profiles with time as the lithiation proceeds following the initial discharge curve in Fig. 3. The particle size was chosen as 40 μm and thus the radial coordinate changes from zero (center of the particle) to 20 μm (surface of the particle). Since the damage at the initial stages of discharge lithiation is close to zero, the portion of the damage surface corresponding to onset of lithiation is not plotted. The intersection of the surface with the damage-radial coordinate planes represents the two dimensional plots of the function $D(r)$ corresponding to different points in time. The intersection of the surface with damage–time plane where damage attains its maximum represents time evolution $D_{max}(t)$ similar to that shown in Fig. 5. The computation continued until the value of $D(r,t)$ reached its maximum and thus the damage profile at the last point in time represents the spatial distribution of damage at the moment of fracture. It can be seen that within the entire time span, the maximum damage occurs at the center of the particle which is where the peak of damage is situated when the cracking initiates. Thus the particle is expected to fracture in the center when the lithium is inserted.

The results reported above are based on the experimental data suggesting that the peak of acoustic emissions occurs during the first discharge; that is most of the particles fracture during the initial insertion of Li. The calculations show rapid increase of the damage and the points of $D = 1$ coincide well with the peaks of acoustic emission (Fig. 6). The predictions are based on the average radius of the particle (50 μm) used in the experiments. At this point it seems only logical to investigate the effect of particle size on damage evolution with time. Once again the loading conditions applied to specimen 48 were used as the input values. The damage–time curves for the particles of three different sizes are

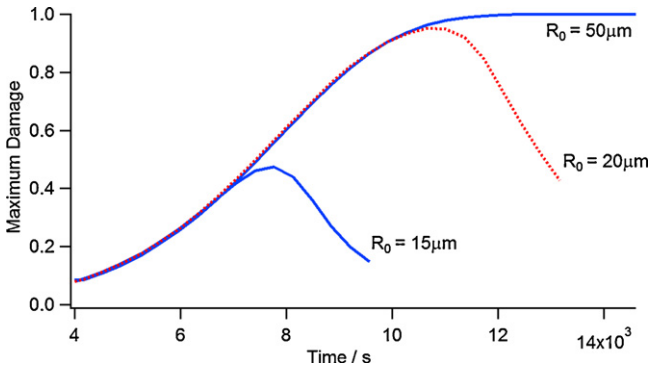

Fig. 8. Distribution of maximum damage for three different radii of Si particle.

shown in Fig. 8. The time period shown in Fig. 8 corresponds to the initial discharge part of the loading curve (Fig. 3). Two trends can be clearly seen from Fig. 8. The value of maximum damage decreases with decrease in particle radius and the time to the peak of the damage also decreases as the particle size is reduced. The former observation is rather intuitive as the larger particle would produce greater stress fields which would lead to fracture. The location of the damage maxima closer to the onset of discharge follows from the fact that the shorter time is needed for lithiation of a smaller particle.

The continued investigation of the size effect is shown in Fig. 9, where the maximum damage and the time until this maximum damage is reached is plotted against the particle radius ranging from 1 to 50 μm. The vertical dashed line represents boundary between two particle sizes identified by the mesh numbers and will be explained in the Discussion section of the paper. It can be seen that as the particle size decreases so does the damage, reaching the limit close to zero for infinitely small particle. The damage then increases rapidly within the range of particle radii between 10 and 20 μm and asymptotically reaches the plateau with the value of 1.0. Finally, it can be seen that for particles smaller than 10 μm in radius the value of damage is rather negligible suggesting that the particles of this range of sizes will not fracture upon the initial discharge. It should be mentioned that the scale of 10 μm is far greater than nanoscale typically considered to be "stress safe" on a single particle level [2,3].

5. Discussion

The present investigation represents the analysis of diffusion induced fracture of Si particles during lithium insertion and extraction based on a working principle of a Li-ion battery. The problem is treated from the continuum mechanics point of view. The prob-

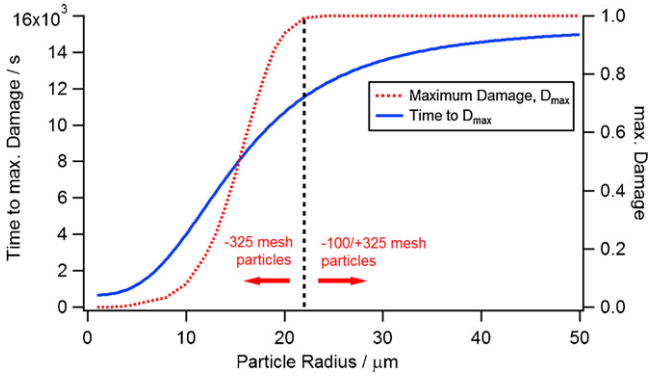

Fig. 9. Damage parameter as a function of particle size.

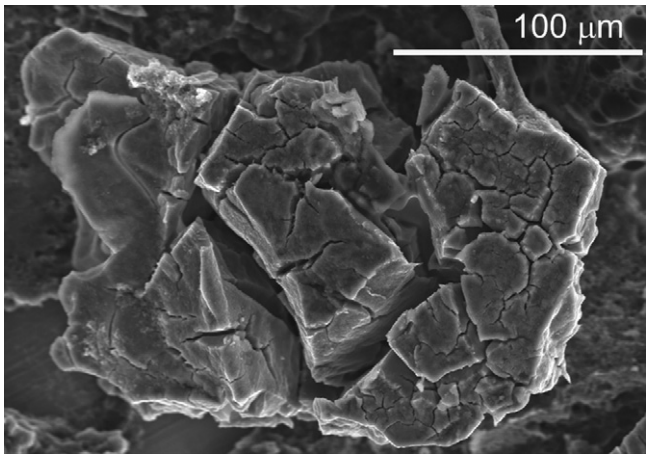

Fig. 10. SEM of a cycled Si particle.

abilistic formalism of deformation analysis of brittle materials resulted in damage parameter reflecting the probability of fracture with $D \rightarrow 1$ representing the prediction of complete failure. Within this notion the stress state is in turn affected by the change in the elastic modulus due to damage following Eq. (19). Distinction between tension and compression is made through consideration of microcracks closure when the stress state is compressive.

Examination of AE data from electrodes tested (Fig. 4) reveals the maximum density of emission events during the first discharge of the cyclic curve. In a half-cell, an anode formally serves as a cathode as it is cycled against lithium metal and thus discharge portion of a cycle represents insertion of Li ions into Si particles. While the highest density of emissions occurs during the first discharge, Fig. 4 shows spikes of emissions during subsequent cycling. The AE events occur during both the discharge, when the stress state on the surface is compressive as well as during charging, when the particle surface stress state is tensile. At the present moment it is rather difficult to make a definite statement as for the cause of subsequent bursts of emissions. It could be suggested that the initial burst of emissions is due to cracking while later on in subsequent cycles the fretting of the existing fracture surfaces and small increments of crack growth can be attributed. Since the examination of electrode material is done ex situ it is impossible to determine the exact sequence of events leading to final fracture of a particle into pieces. The continuation of the current research will be done by in situ optical microscopy using a specially designed Li half cell. Such in situ observations will give valuable information regarding development of cracking with electrochemical cycling.

An example of cycled particle is shown on SEM image in Fig. 10. Multiple cracks separating the particle into smaller blocks can be observed, however the location of crack initiation cannot be deducted from this picture. It is quite possible that the cracking during the initial discharge started from the center of the particle where the prediction places the maximum of the damage parameter (Fig. 7) separating the particle into several blocks. Subsequent charge would introduce the surface cracks in those blocks producing the burst of emissions corresponding to the charging part of the cycle. Then during the next discharge the internal cracks would appear again and so on, until the block reaches a critically small size to develop enough stress for fracture. The geometry of the internal crack produced during the first discharge depends on the distribution of initial internal defects in the particle and is impossible to predict within the generalized homogeneous spherical body approach. In other words it is impossible to quantify the amount of blocks produced by initial fracture of a particle.

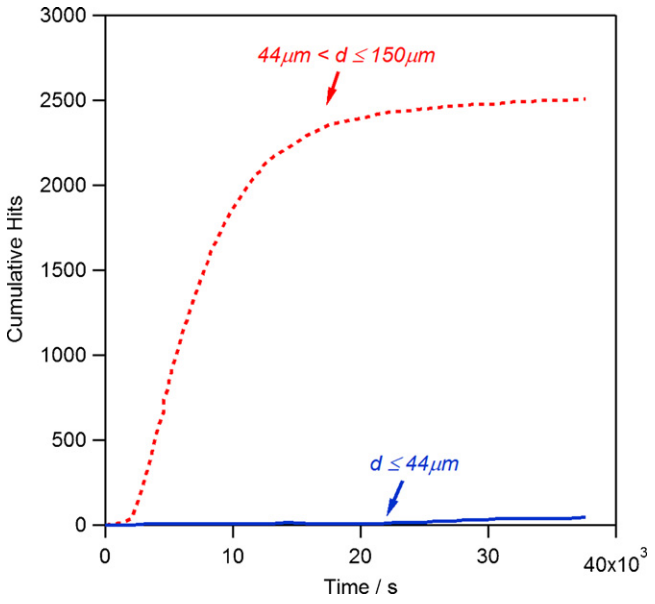

Fig. 11. Comparison between AE cumulative events from two different particle size distributions.

Investigation of the particle size effect on the evolution of damage produces the result which reveals the existence of particle size range, for which the value of maximum damage is less than 1 (Fig. 9). Additional examination of Fig. 9 yields observation that as the particle radius comes close than 10 μm the damage becomes negligibly small. The particle size in the vicinity of 10 μm in radius thus can be considered as fracture safe under the current cycling conditions.

It should be mentioned that the above size range is still much larger than expected in the electrochemical community where the shift towards nano-sized electrode particles is considered to be one of the solutions for extension of battery life [2,3,40]. The benefits of nanoscopic materials for lithium battery applications consist of short diffusion distances, which implies increase in rate capability, and large surface areas, which allows for fast absorption of lithium ions [3]. Less severe concentration gradients inside smaller particles result in reduced magnitude of stress which prevents fracture. It has been reported that reduction of $LiMn_{1.5}Ni_{0.5}O_4$ particle size from 1 μm to 70 nm resulted in significant improvement in capacity retention [41]. Work on nano-structured arrays of Si pillars (~600 nm in diameter) showed that at this length scale the material maintained its structural integrity during electrochemical cycling [42]. The results of current investigation suggest that prevention of cracking may be achieved in particles with size much larger than the nanometer region.

In order to validate the size effect shown in Fig. 9, one of the electrodes was prepared with Si particles of −325 mesh, that is less than 22 μm in radius. The electrode was cycled between 1.3 V and 50 mV with 0.53 mA current amplitude. The results are shown in Fig. 11 and compared to the AE results from the electrode with −100/+325 mesh particles (average radius 50 μm) cycled under the same conditions. According to ASTM-E11 standard, the mesh numbers are used in description of sizes of particulate materials and denote the sieve openings through which particles are passed. The sign in front of the number corresponds to whether particles go through the sieve or are trapped. In our case, the designation −325 mesh indicates that particles smaller than 44 μm will pass through the sieve, and designation −100/+325 means that particles will pass through 150 μm openings (−100) but will be stopped by 44 μm sieve (+325). The line corresponding to particle diameter of 44 μm and thus demarcating the two meshes is placed in Fig. 9 in order to distinguish the corresponding values of damage. It can be seen in Fig. 9 that the part of the maximum damage curve corresponding to the particles smaller than 44 μm is distinguished by the abrupt drop in values of damage parameter, while for the particles larger than 44 μm the damage approaches the asymptotic maximum value of unity. Confirming the predictions from Fig. 9, Fig. 11 shows that the number of hits registered in the small-particle electrode is magnitudes less than in the case of 50 μm particles. The experimental work, which targets investigation of size effect on fracture time, is under way and should further reveal the dependence of damage on particle size as well as demonstrate the existence of critical size following the computational results presented in current manuscript.

6. Conclusions

The problem of Si particles fracture upon insertion of lithium in a Li-ion half-cell was treated within the continuum mechanics approach with brittle damage parameter. The results predict fracture upon the immediate first discharge and are in agreement with experimental acoustic emissions data obtained from charge/discharge cycling of a half cell with Si as anode active material. Consideration of particle size effect on developed chemical stresses suggests a critical size of a particle which would not fracture upon initial lithiation. Such critical size appears to be within micrometer scale.

Acknowledgements

This research at Oak Ridge National Laboratory, managed by UT Battelle, LLC, for the U.S. Department of Energy under contract DE-AC05-00OR22725 was sponsored by the Vehicle Technologies Program for the Office of Energy Efficiency and Renewable Energy. Parts of this research were performed at the High Temperature Materials Laboratory, which is a user facility sponsored by the same office.

The United States Government retains, and the publisher, by accepting this submission for publication, acknowledges that the United States Government retains, a nonexclusive, paid-up, irrevocable, worldwide license to publish or reproduce the published form of this submission, or allow others to do so, for United States Government purposes.

References

[1] J.O. Besenhard, Handbook of Battery Materials, Willey-VCH, 1998.
[2] C. Daniel, JOM 60 (9) (2008) 43–48.
[3] A.K. Shukla, T.P. Kumar, Curr. Sci. 94 (3) (2008) 314–331.
[4] P. Arora, R.E. White, M. Doyle, J. Electrochem. Soc. 145 (10) (1998) 3647–3667.
[5] J. Christensen, J. Newman, J. Solid. State Electrochem. 10 (2006) 293–319.
[6] Y. Shao-Horn, S.A. Hackney, A.J. Kahaian, K.D. Kepler, E. Skinner, J.T. Vaughey, et al., J. Power Sources 81/82 (1999) 496–499.
[7] Y. Shin, A. Manthiram, Electrochem. Solid State Lett. 5 (3) (2002) A55–A58.
[8] D. Wang, X. Wu, Z. Wang, L. Chen, J. Power Sources 140 (2005) 125–128.
[9] K.Y. Chung, K.B. Kim, J. Electrochem. Soc. 149 (1) (2002) A79–85.
[10] F. Yang, Mater. Sci. Eng. A 409 (1–2) (2005) 153–159.
[11] X. Zhang, W. Shyy, A.M. Sastry, J. Electrochem. Soc. 154 (10) (2007) A910–916.
[12] Y.T. Cheng, M.W. Verbrugge, J. Power Sources 190 (2009) 453–460.
[13] M.W. Verbrugge, Y.T. Cheng, J. Electrochem. Soc. 156 (11) (2009) A927–937.
[14] J. Christensen, J. Newman, J. Solid State Electrochem. 10 (2006) 293–319.
[15] J. Christensen, J. Newman, J. Electrochem. Soc. 153 (6) (2006) A1019–1030.
[16] H.H. Chiswick, Trans. Am. Soc. Metals 49 (1957) 622–654.
[17] L.F. Coffin Jr., Trans. ASME 76 (6) (1954) 931–950.
[18] S.S. Manson, Thermal Stress and Low Cycle Fatigue, McGraw-Hill, 1966.
[19] Y. Jiang, Fatigue Fract. Eng. Mater. Struct. 23 (2000) 19–32.
[20] C.-C. Chu, J. Eng. Mater. Technol. ASME 117 (1995) 41–49.
[21] G. Glinka, G.A. Shen, Fatigue Fract. Eng. Mater. Struct. 18 (1995) 37–46.
[22] R.O. Ritchie, Int. J. Fract. 100 (1999) 55–83.
[23] A. George, A. Jacques, M. Legros, Fatigue Fract. Eng. Mater. Struct. 30 (2007) 41–56.
[24] S. Timoshenko, J.N. Goodier, Theory of Elasticity, McGraw-Hill, 1951.

[25] O.M. Jadaan, N.N. Nemeth, J. Bagdahn, W.N. Sharpe Jr, J. Mater. Sci. 38 (2003) 4087–4113.
[26] J. Lemaitre, R. Desmorat, Engineering Damage Mechanics. Ductile, Creep, Fatigue and Brittle Failures, Springer-Verlag, Berlin, Heidelberg, 2005.
[27] ASTM C1239-07, Standard practice for reporting uniaxial strength data and estimating Weibull distribution parameters for advanced ceramics, ASTM International February 1, 2007.
[28] F. Hild, P.L. Larsson, F.A. Leckie, Compos. Struct. 29 (1994) 365–377.
[29] D. Krajcinovic, A.M.G. Silva, Int. J. Solid Struct. 18 (7) (1982) 551–562.
[30] M.N. Obrovac, L.J. Krause, J. Electrochem. Soc. 154 (2) (2007) 103–108.
[31] K. Rhodes, N. Dudney, E. Lara-Curzio, C. Daniel, J. Electrochem. Soc. 157 (12) (2010) A1354–1360.
[32] H. Inoue, R. Tsuzuki, S. Nohara, C. Iwakura, Electrochem. Solid-State Lett. 9 (11) (2006) A504–506.
[33] H. Inoue, R. Tsuzuki, S. Nohara, C. Iwakura, J. Alloys Compd. 446/447 (2007) 681–686.
[34] S. Didier-Laurent, H. Idrissi, L. Roue, J. Power Sources 179 (1) (2008) 412–416.
[35] R. Hull, Properties of Crystalline Silicon, INSPEC Publication, London, UK, 1999.
[36] T.L. Kulova, A.M. Skundin, Yu.V. Pleskov, E.I. Terukov, O.I. Kon'kov, J. Electroanal. Chem. 600 (1) (2007) 217–225.
[37] M. Suzuki, J. Suzuki, K. Sekine, T. Takamura, J. Power Sources 146 (2005) 452–456.
[38] N. Ding, J. Xu, Y.X. Yao, G. Wegner, X. Fang, C.H. Chen, et al., Solid State Ionics 180 (2009) 222–225.
[39] M. Winter, J.O. Besenhard, Acta Electrochim. 45 (1–2) (1999) 31–50.
[40] C. Wang, A.J. Appleby, F.E. Little, J. Power Sources 93 (2001) 174–185.
[41] M. Kunduraci, G.G. Amatucci, Electrochim. Acta 53 (2008) 4193–4199.
[42] M. Green, E. Fielder, B. Scrosati, M. Wachtler, J. Serra Moreno, Electrochem. Solid State Lett. 6 (5) (2003) A75–A79.